

1 **Petrogenesis of Alkalic Seamounts on the Galápagos Platform**

2

3 Darin M. Schwartz^a *darinschwartz@boisestate.edu*, V. Dorsey Wanless^a, Rebecca Berg^a,

4 Meghan Jones^b, Daniel J. Fornari^b, S. Adam Soule^b, Marion L. Lytle^a, Steve Carey^c

5

6 ^a Department of Geosciences, Boise State University, 1910 University Drive, Boise, ID

7 83725

8 ^b Geology and Geophysics Department, Woods Hole Oceanographic Institution

9 ^c Graduate School of Oceanography, University of Rhode Island

10

11 **Keywords: seamounts, geochemistry, monogenetic, hotspot, Galápagos, basalt, E/V**

12 *Nautilus*

13

14

15

16

17

18

19

20

21

22

23

24

25

26

27

28

29

30

31

32

1

2 **Abstract**

3 In the hotspot-fed Galápagos Archipelago there are transitions between volcano
4 morphology and composition, effective elastic thickness of the crust, and lithospheric
5 thickness in the direction of plate motion from west to east. Through sampling on the
6 island scale it is unclear whether these transitions are gradational or sharp and whether
7 they result in a gradational or a sharp boundary in terms of the composition of erupted
8 lavas. Clusters of interisland seamounts are prevalent on the Galápagos Platform, and
9 occur in the transition zone in morphology between western and eastern volcanoes
10 providing an opportunity to evaluate sharpness of the compositional boundary resulting
11 from these physical transitions. Two of these seamounts, located east of Isabela Island
12 and southwest of the island of Santiago, were sampled by remotely operated vehicle in
13 2015 during a telepresence-supported E/V *Nautilus* cruise, operated by the Ocean
14 Exploration Trust. We compare the chemistries of these seamount lavas with samples
15 erupted subaerially on the islands of Isabela and Santiago, to test whether seamounts are
16 formed from melt generation and storage similar to that of the western or eastern
17 volcanoes, or transitional between the two systems. There are no systematic variations
18 between the two seamounts and variability in all samples can be related through <10%
19 fractional crystallization at 500-900 MPa. Both seamounts are interpreted to represent a
20 single magmatic episode and eruptive event. Trace element compositions indicate they
21 formed downstream of the hotspot center. The calculated extents of melting are
22 consistent with generation of magmas sourcing the seamounts beneath lithosphere of
23 intermediate thickness (~56 km). The seamount lavas have compositions that are nearly
24 identical to a subset of lavas erupted subaerially on Santiago Island, suggesting lateral
25 magma transport on the order of 10 km from their source region prior to eruption. The
26 compositional characteristics and, in particular, depth of crystallization suggest that
27 although seamount magmas have a transitional melting signature, they are discretized on
28 the island scale, through homogenization in the lithospheric mantle and redistributed by
29 vertical and horizontal diking in the shallow crust. Due to this homogenization, it remains
30 unclear whether the variation in erupted lava chemistries from west to east are
31 representative of sharp or gradual changes in mantle composition and structure across the
32 archipelago.

1

2 **1. Introduction**

3 The lifespan of hotspot sourced volcanic islands is controlled by the interplay
4 between volcano growth (i.e., eruption rate), subsidence and erosion (e.g., Geist et al.,
5 1996; 2014a). These processes are modulated by the transport of the islands away from a
6 fixed “plume” source by plate motion (e.g., Morgan, 1972). The archetypal example of
7 this process is the Hawaiian Island chain. The Hawaiian Islands form a linear, age-
8 progressive, volcanic succession parallel to the direction of absolute plate motion, where
9 large, young islands become progressively smaller, older and more dissected to the
10 northwest (e.g., Clague and Dalrymple, 1987). This general progression is less clear for
11 other plume-sourced intraplate volcanic systems, including the Galápagos Archipelago,
12 which is the subject of this study (Fig. 1).

13 The Galápagos consists of 13 major volcanic islands and numerous smaller
14 islands, and volcanic seamounts in the eastern equatorial Pacific (Fig. 1; McBirney and
15 Williams, 1969, Christie et al., 1992). Most of the islands rise from a large (~3500 km²),
16 shallow volcanic platform that stands ~3000 m above the surrounding seafloor (Geist et
17 al., 2008a). The center of plume upwelling in the Galápagos lies southwest of Fernandina
18 Island, the westernmost and most active volcano (Allan and Simkin, 2000). The position
19 of the plume source has been inferred based on a locally thin mantle transition zone (Fig.
20 1; Hooft et al., 2003), low shear-wave velocities (Villagómez et al., 2007; 2011), and
21 geochemical enrichment (e.g., Kurz and Geist, 1999). Although there is a general age
22 progression akin to that of Hawaii (White et al., 1993), the Galápagos differs from
23 Hawaii in the persistence of volcanic activity up to 250 km away from the inferred plume
24 center (e.g., Geist et al., 1986), and a wide distribution of islands and seamounts towards
25 the Galapagos Spreading Center, attributed to plume ridge interaction (Harpp and Geist
26 2002; Harpp et al., 2003). Despite continued volcanism away from the locus of mantle
27 upwelling, there are clear differences in the magmatic plumbing systems between the
28 western and eastern volcanoes in the Galápagos.

29 The Galápagos Archipelago displays a unique, systematic variation in
30 morphology between the volcanoes in the west compared to those in the east. The
31 western islands (Fernandina and Isabela; Fig. 1) are typified by the presence of large and
32 multicyclic summit calderas, surrounded by circumferential fissures near the summits and

1 radial vents on the flanks (Chadwick and Howard, 1991), which are indicators of the
2 presence of persistent shallow (~2 km; Yun et al., 2006, Geist et al., 2008b, Geist et al.,
3 2014b) magma chambers and periodic eruption cycles (Chadwick and Dieterich, 1995).
4 The western volcanoes typically erupt homogenous tholeiitic lavas, resulting from
5 primarily shallow (200 MPa; Geist et al., 1998) crystal fractionation (<7 % MgO; e.g.,
6 Saal et al., 2007). By contrast, older islands to the east (Santiago, Santa Cruz, San
7 Cristobal, Floreana, and satellite islands; Fig. 1) are broad shields that generally lack
8 calderas, and are dominated by flank eruptions, spatter or cinder cones, and elongate rift
9 zones that extend from the island summit to the lower subaerial flanks (e.g., Swanson et
10 al., 1974; Geist and Harpp, 2009). The lavas erupted on the eastern islands and in the
11 central archipelago (e.g., Santiago; Santa Cruz) are highly variable in composition, with
12 rock types ranging from picrites to trachytes (McBirney and Williams 1969; Swanson et
13 al., 1974; Saal et al., 2007; Herbert et al., 2009; Gibson et al., 2012; Wilson, 2013) and
14 have signatures of deep crystal fractionation (600-900 MPa; Geist et al., 1998).

15 This transition between western and eastern volcano morphology is mirrored by a
16 transition in both the effective elastic thickness of the crust from 12 km in the west to 6
17 km in the east (Feighner and Richards, 1994) and lithospheric thickness from 70 km in
18 the west to 40 km in the east (Villagómez et al., 2007). The change in lithospheric
19 thickness ultimately affects the total extent of mantle melting and therefore magma
20 compositions produced in each region (Fig. 1; Gibson and Geist, 2010). However,
21 because sampling has been restricted primarily to the subaerial islands, it is unclear
22 whether the crustal and lithospheric thickness variations and resulting geochemical
23 signals are abrupt or gradational across the archipelago.

24 In 2015, we explored and sampled two seamounts that lie between Isabela in the
25 west and Santiago, which presently erupt as caldera-forming and dispersed styles. The
26 seamounts are within the transition between thin and thick lithosphere (e.g., Villagómez
27 et al., 2007) to determine if there are systematic changes in lava compositions that
28 correlate with geophysical transitions. Specifically, the seamounts are located between
29 Isabela in the west and Santiago in the eastern region of the archipelago (Fig. 1). We
30 present the first suite of geochemical data from these seamounts with twelve samples
31 collected by the remotely operated vehicle (ROV) *Hercules*. Analyses of these samples
32 (major and trace element concentrations and volatile contents) provide the first direct

1 measurements of interisland volcanic activity in the modern archipelago. We use these
2 samples to 1) determine depths of crystallization and compositional heterogeneity
3 beneath the seamounts, 2) compare the chemical characteristics of the seamounts to those
4 of the adjacent western and eastern volcanic islands, and 3) test whether the seamounts
5 are formed through magma delivery from a distinct deep magmatic source directly below
6 the seamounts, or from a magma reservoir that also feeds an adjacent volcanic island.

8 **2. Remotely operated vehicle (ROV) dives and sample collection**

9 Rock samples were collected in collaboration with the Ocean Exploration Trust
10 on the *E/V Nautilus* cruise NA064 in July 2015 using the ROV *Hercules* (Bell et al.,
11 2016). Dive planning and sample collection was coordinated via telepresence from the
12 Woods Hole Oceanographic Institution's Exploration Command Center. Instructions to
13 the onboard team of engineers and scientists were provided via satellite link using both
14 voice, text-based chat, and video links, with real-time data transmitted from the ROV.
15 The dive traversed two unnamed seamounts southwest of Santiago (Fig. 2) and collected
16 15 rock samples (seven analyzed from the northern seamount and five analyzed from the
17 southern seamount; Table 1), in addition to extensive high definition video footage and
18 digital still imagery (Carey et al., 2016). While nearby seamounts observable in the
19 existing Galápagos multibeam bathymetry are nearly conical in shape (Fig. 2), both
20 seamounts explored during this cruise are more complex, consisting of a central dome of
21 pillow lavas flanked by a semicircular ring of volcanoclastic sediment and talus.

23 *2.1 Northern seamount description*

24 The northern seamount has a diameter of 1.6 km is 263 m tall, and has a volume
25 of 0.14 km³ (Fig. 2). The base of the seamount lies at 645 m depth and the shallowest
26 point on the eastern summit is at 381 m depth. The summit consists of a horseshoe
27 shaped crater rim, open to the west, composed predominately of volcanoclastic sediment,
28 with a small summit depression containing a lava dome or flow in its center. A N-S linear
29 volcanic ridge extends south from the seamount.

30 The outer slopes of the seamount are comprised predominately of unconsolidated,
31 tan sediment at the base of the seamount with increasing proportions of, volcanoclastic,
32 black sediment towards the top. The seamount has upper flank slopes that average 23°,

1 with sparse cobbles or boulders of volcanic rock that increase in size with shallower
2 depths. No *in situ* lava flows were observed or sampled on the volcano flanks, but two
3 loose rocks, heavily coated with biological material, were collected from the upper third
4 of the exterior (NA064-113) and interior (NA064-114) slopes. Within the summit
5 depression a small dome or lava flow stands ~ 20 m above the surrounding seafloor. The
6 dome flow is composed almost entirely of basaltic lava, lightly dusted with sediment. The
7 morphology of the flow ranges from intact and broken pillows to hackly or jumbled lava.
8 Two *in situ* samples were collected from this outcrop (NA064-115 and 116).

9 The linear volcanic ridge extending south of the crater is ~0.5 km long and
10 consists of three small mounds (decreasing in elevation to the south). The tops of the
11 three mounds are composed of relatively large intact pillow lavas, while the lower slopes
12 consist of lavas and sediment. The linear ridges connecting the mounds are composed of
13 smaller pillow tubes with minor volcanic sediment. Lava samples NA064-120 and
14 NA064-123 were collected from the first mound and samples NA064-127 and NA064-
15 129 were collected from the top of the two smaller mounds to the south (Fig. 2).

17 2.2 Southern seamount description

18 The larger southern seamount has diameter of ~ 3 km, a height of 388 m, and a
19 volume of 0.34 km³ (Fig. 2). The base of the seamount lies at 653 m depth and the
20 shallowest point is at 265 m depth. The summit is located at the center of the seamount
21 and is composed of spatter and pillow lavas. Upper flank slopes average ~18° and are
22 composed of unconsolidated sediment and a few sparse cobbles. The semi-circular flank
23 is open to the southwest.

24 The slopes and crater rim of the seamount are composed almost entirely of tan
25 sediment, with very sparse boulders of volcanic rock. One loose sample was collected
26 from the northern rim of this seamount (NA064-132). The central peak is composed of
27 loose pebble- to cobble-sized basaltic material, which bears resemblance to subaerial
28 spatter (Sample NA064-131). The only intact lava observed on this seamount is a pillow
29 and hackly lava flow that originates near the peak of the central dome and flows
30 downslope to the north. One sample of this lava flow was collected (NA064-133). Two
31 samples (NA064-134 and 135) were collected from heavily sedimented seafloor west of
32 the seamount.

1

2 **3. Geochemical methods**

3 Samples were crushed using a mechanical jaw crusher at Boise State University.
4 Crushed rock chips were rinsed in an ultrasonic bath using a 1% hydrogen peroxide
5 solution, followed by DI water until clean. Approximately 1–2 mm-sized cleaned chips
6 were handpicked using a binocular microscope, avoiding phenocrysts and alteration.
7 Oxidized surfaces were unavoidable on two heavily altered samples (115 and 120).

8 Whole rock major and select trace element contents were analyzed using a
9 Thermo-ARL automated X-ray Fluorescence (XRF) spectrometer at Washington State
10 University (Table 2). Clean chips (25–50 g) were powdered using a ring mill with
11 tungsten carbide surfaces and fused with Li-tetraborate into glass beads for analyses,
12 following methods of Johnson et al. (1999). Sample NA064-115 was run with a repeat
13 bead to assess procedural reproducibility, which is $\leq 1\%$ difference for all elements; these
14 two analyses were averaged.

15 Whole rock trace element contents were analyzed by solution ICP-MS at Boise
16 State University following the procedures of Kelley et al. (2003) and Lytle et al. (2012)
17 (Table 3). Approximately 50 mg of each sample were digested in closed 23 mL Savillex
18 Teflon beakers in 3 mL of 8N HNO₃ and 1 mL of HF. Sealed capsules containing
19 sample-acid solution were placed on a hot plate at $\leq 100^\circ\text{C}$ overnight (~12 hours) until no
20 trace of solids remained. Dissolved samples were then evaporated to dryness, uncapped
21 on a hot plate, keeping surface temperature $\leq 100^\circ\text{C}$, and then re-dissolved in 3 mL of 8N
22 HNO₃ and 3 mL of ultra-pure de-ionized H₂O in sealed capsules on a hot plate at $\leq 100^\circ\text{C}$
23 for ~12 hours. The dissolved samples were transferred into 125 mL HDPE bottles for a
24 2500x ultra-pure water dilution and sonicated for 30 minutes to ensure dissolution of all
25 precipitates. Trace element concentrations were measured using a Thermo Electron X-
26 Series II Quadrupole Inductively Coupled Plasma Mass Spectrometer (ICP-MS) coupled
27 with an ESI SC-FAST autosampler. Samples were corrected using an internal standard
28 solution containing In, blank corrected using a procedural blank, drift corrected using
29 Geological Survey of Japan (GSJ) standard JB-3, dilution weight corrected, calibrated
30 using US Geological Survey (USGS) standards, GSJ standards, and internal laboratory
31 standards: BHVO-2, BIR-1, DNC-1, W-2 (USGS), JB-3 (GSJ), and 2392-9 (University
32 of Florida in-house standard; Goss et al., 2010). Trace element concentrations for each

1 sample are reported as the mean of three individual analyses, the precision is reported as
2 the standard deviation of these analyses (supplementary data tables).

3 Only one sample had glass suitable for volatile analyses. Volatile contents were
4 measured on a glass chip from sample NA064-114 using the Cameca 1280 Secondary Ion
5 Mass Spectrometer at Northeast National Ion Microprobe Facility (NENIMF) at the
6 Woods Hole Oceanographic Institution, using a Cs⁺ beam with a 30 μm raster size, field
7 aperture of 1250 μm and entry slit of 81 μm, following methods by Hauri et al. (2002;
8 Table 2). The glass fragment was hand-polished using a range of grits on silica carbide
9 sandpaper, mounted in indium, and polished at 6, 3, and 1 μm diamond polish and 1 μm
10 alumina grit for 5-30 minutes each. Volatile standard 519-4-1 (Hauri et al., 2002) was
11 measured routinely throughout the session to monitor for instrumental drift.

12 Measurements were calibrated with a known set of standard glasses provided by the
13 NENIMF.

14 15 **4. Results**

16 Samples from both seamounts have vesicularities on the order of 50%. All
17 samples contain 1-3%, ~1 mm plagioclase and olivine phenocrysts, with the exception of
18 sample 131, which has ~7% olivine phenocrysts that are up to 2 mm. Major element
19 contents are reported in Table 2. All of the samples are relatively mafic basalts, with
20 MgO contents ranging from 7.74 to 9.42 wt% (Fig. 3). The degree of alteration observed
21 in hand samples correlates with high loss on ignition (LOI; Table 2). Samples with LOI
22 >1% greatly increase the variability of major elements including FeO_T, P₂O₅, CaO and
23 Na₂O (Fig. 3). Excluding sample 115, which is the most pervasively altered (2.38 wt%
24 LOI), most of the major elements have relatively limited variability, with Al₂O₃ ranging
25 from 15.31-16.07 wt%, TiO₂ from 2.18-2.44 wt%, Na₂O from 2.52–2.96 wt%, and K₂O
26 from 0.34 to 0.46 (Fig. 3). There is slightly higher variability in CaO (9.10-11.95 wt%)
27 and FeO_T (11.35-12.85 wt%). CaO/Al₂O₃ ratios range from 0.60 to 0.78 (Fig. 4). The
28 basalts are all mildly alkalic, with total alkali contents (Na₂O + K₂O) ranging from 3.06-
29 3.35 and SiO₂ contents of 44.64–46.80 wt% (Fig. 3).

30 Trace element contents are reported in Table 3, uncertainties are reported in the
31 supplementary data tables. Samples from both seamounts span a narrow range in
32 incompatible trace element concentrations (e.g., 13-15 ppm Nb, 56-65 ppm Ba; Fig. 5).

1 Despite the slight variations in concentration, the samples have low variability in CI
2 chondrite normalized (McDonough and Sun, 1995) trace element ratios (e.g., [La/Nb]_N
3 0.74-0.77; Fig. 6). REE patterns are nearly uniform for all samples, with a negative slope
4 at increasing atomic mass and slight concave down pattern in light REEs (Fig. 7). REE
5 ratios are also similar (e.g., [La/Sm]_N 1.3-1.4[Sm/Yb]_N 2.1-2.5; Fig. 8). All samples show
6 a broad increase in primitive mantle normalized trace element concentrations with
7 increasing incompatibility, save for the most incompatible elements, Rb and Ba, which
8 are depleted relative to more compatible Th and Nb (Fig. 5).

9 Glass from sample NA064-114 was measured for H₂O, CO₂, Cl, F, and S. The
10 sample has a H₂O concentration of 0.87 wt. %, a CO₂ concentration of 135 ppm, Cl
11 concentration of 210 ppm, F concentration of 891 ppm, and S concentration of 1636 ppm
12 (Table 2). All samples have high vesicularities, on the order of 50%, so significant
13 degassing likely occurred prior to eruption.

14 15 **5. Petrogenesis**

16 Major element variability and slight negative slopes in incompatible minor
17 elements (TiO₂, K₂O, P₂O₅) with MgO (Fig. 3) suggest all seamount lavas sampled from
18 these seamounts are related through small extents of fractional crystallization. To test this
19 hypothesis and assess the mean depth of crystallization, we modeled fractional
20 crystallization using alphaMELTS (Ghiorso and Sack, 1995; Asimow and Ghiorso, 1998,
21 Smith and Asimow, 2005). Crystallization models were run at 100, 500 and 900 MPa,
22 QFM buffered, log Δ*f*O₂ offset of -0.83 (average Galápagos basalt; Rilling, 2005),
23 primitive starting composition (taken from Santa Cruz; Wilson, 2013) and water contents
24 of 0.87 wt. % (based on volatile contents in quenched glass from sample NA064-114).
25 This water content is near the upper limit for submarine basaltic glasses analyzed in the
26 Galápagos (0.098-1.15 wt. % H₂O; Peterson et al., 2013) but is likely a lower bound
27 given the high vesicularities in these samples.

28 Results of the petrologic models suggest that the range of major element
29 compositions at both seamounts can be explained by <10% crystallization of
30 olivine+clinopyroxene from a similar parental magma (Fig. 4), and that the majority of
31 lavas are related by ~4% fractional crystallization. Notably, sample NA064-115 is offset
32 from many of the crystallization trends (FeO_T, K₂O, and P₂O₅), which likely results from

1 significant alteration (LOI = 2.38%) of the whole rock. The best-fit trends were produced
2 from crystallization at pressures between 500-900 MPa. Crystallization paths between the
3 north and south seamounts are offset in $\text{CaO}/\text{Al}_2\text{O}_3$ as a function of Mg# (molecular
4 $\text{MgO}/(\text{MgO}+\text{FeO}_T)\times 100$), which may indicate magma storage and crystallization at
5 variable depths prior to eruption or crystallization during ascent (Fig. 4). In either case,
6 these models suggest that the seamount lavas underwent storage and minor crystallization
7 in a deep (17-35 km) magma chamber. This is significantly shallower than the inferred
8 base of the lithosphere in the region (~55 km; Villagómez et al., 2007; Gibson et al.,
9 2012), but is deeper than crustal thickness estimates for the central archipelago (~16 km;
10 Feighner and Richards, 1994; Toomey et al., 2001). Thus, these depths imply
11 crystallization in the lithospheric mantle.

12 Lavas from both seamounts show slight variations in trace element concentrations
13 (e.g., 9.38-10.99 ppm La; Fig. 6). These variations can be produced by fluctuations in
14 extents of partial melting (Shaw, 1970), source variation (e.g., Weaver, 1991), or
15 fractional crystallization (Shaw, 1970). Variations in extents of partial melting or mantle
16 sources with different trace element concentrations will result in differences in trace
17 element ratios (e.g., low extents of melting or mixing with an enriched source will
18 produce high La concentrations and high $[\text{La}/\text{Sm}]_N$ ratios or low $[\text{La}/\text{Nb}]_N$ ratios; e.g.,
19 Kurz and Geist, 1999). By contrast, limited extents of fractional crystallization, such as
20 those indicated by major element variations (<10%; Fig. 4) will result in nearly equal
21 enrichments of all incompatible trace elements, preserving trace element ratios. Despite
22 limited variations in trace element concentrations at both seamounts, there are only minor
23 variations in $[\text{La}/\text{Sm}]_N$ and no variation in $[\text{La}/\text{Nb}]_N$ (Figs. 6, 8), indicating that the lavas
24 may be produced by only slight variations in degree of melting of a similar source. The
25 nearly uniform trace element ratios (Figs. 6, 8) and REE patterns (Fig. 7) are consistent
26 limited fractional crystallization during the evolution of magmas at both seamounts.

27 White et al., (1993) noted a downstream depletion in highly incompatible trace
28 elements from the center of plume upwelling, attributed to progressive dilution of the
29 mantle plume with entrained upper mantle material. The primitive component of the
30 Galápagos mantle plume has can be identified by high $^3\text{He}/^4\text{He}$ isotopic ratios (~30 Ra,
31 Kurz and Geist, 1999; Kurz et al., 2009), which correlates with elevated Ti, Ta and Nb,
32 relative to elements of similar compatibilities (Kurz and Geist, 1999, Jackson et al.,

1 2008). This dilution trend is manifested as extremely low $[La/Nb]_N$ ratios in lavas erupted
2 at Fernandina compared to nearby Wolf, Darwin and Alcedo volcanoes on Isabela Island
3 (Fig. 6; mean $[La/Nb]_N$ 0.67 and 0.97, respectively), despite similar degrees of melting
4 predicted for this region (Gibson and Geist, 2010). The downstream change in these
5 ratios allows us to assess the lateral position of melt generation that produced the
6 seamounts relative to the plume center. Seamount lavas have mean $[La/Nb]_N$ 0.75 (Fig.
7 6), which is higher than that of lavas erupted at Fernandina. This suggests that the
8 seamounts did not form over the plume center and migrate eastward with plate motion,
9 but instead erupted relatively recently downstream of the plume center.

10 The dissolved CO_2 concentration measured in sample NA064-114 (135 ppm) is
11 ~95% less than presumably undegassed Galápagos melt inclusion contents (up to 5821
12 ppm CO_2 ; Koleszar et al., 2009). This concentration is also much lower than the range of
13 CO_2 (4200-5600 ppm) predicted from CO_2/Nb for undegassed mid-ocean ridge basalts
14 (300; Saal et al., 2002) and Galápagos lavas (400; Peterson et al., 2013) using mean Nb
15 values of the seamount samples (14 ppm). By contrast, S (1636 ppm) is comparable to
16 that of S measured in undersaturated submarine glasses collected at greater water depths
17 (1599 ppm; Peterson et al., 2010). Despite evidence for extensive degassing (high
18 vesicularities), the CO_2 contents are still greater than predicted for their eruption depths.
19 Any excess volatile concentrations, relative to experimentally derived solubility curves,
20 likely result from rapid ascent and quenching with insufficient time for degassing (e.g.,
21 Dixon et al., 1988; le Roux et al., 2006). We use the dissolved CO_2 and H_2O
22 concentrations measured in NA064-114 (135 ppm and 0.87 wt. %, respectively) to yield a
23 vapor saturation pressure of 36 MPa, which is equivalent to ~1.2 km below seafloor
24 (Dixon and Stolper, 1995; Newman and Lowenstern, 2002). Thus, we suggest that the
25 exsolution of CO_2 and H_2O , within a magmatic system at >1.2 km depth drove rapid
26 magma ascent, vesiculation and fragmentation. Fragmentation may also be enhanced by
27 seawater interaction, common for submarine volcanoes at depths between 200-1300 m
28 (Allen and McPhie, 2009). This is consistent with pyroclastic activity forming a majority
29 of the volume of each seamount edifice, followed by limited extents of effusive
30 volcanism associated with crater filling pillow lava and flows.

31 The similarity between the two seamounts in major elements (Fig. 3), trace
32 element contents (Fig. 5) and ratios (Figs. 6, 8) indicates that they were either produced

1 from the same mantle source and evolved under similar conditions or shared the same
2 batch of magma and were erupted over a short duration. Similarity in morphological
3 features between the two seamounts, including outer slope angles and southwestward
4 breaching, indicates similarity in vent conditions and ocean currents during eruption (e.g.,
5 Settle, 1979). Combined with the spatial proximity of the two seamounts, we suggest
6 that, together, the seamounts were produced during a single eruptive event or closely
7 timed events originating from the same magma batch. Individual seamount volumes
8 (0.14-0.36 km³) are on the order of other single lava flows observed in the Galápagos
9 (0.12 km³; Rowland, 1996), and combined are less than the total volume for single
10 eruptive events described for multiple events at Fernandina (2 km³; Simkin and Howard,
11 1970; 2.3 km³; Rowland, 1996), thus it is conceivable that both were produced from a
12 single monogenic basaltic eruption.

13

14 **6. Comparison of seamounts to the western and eastern volcanic systems on the** 15 **Galápagos Platform**

16 *6.1. Extents of melting and lithospheric thickness*

17 The mean extent of melting experienced by the upwelling mantle beneath a
18 hotspot volcano is controlled by the depth difference between the solidus and the base of
19 the lithosphere (e.g., McKenzie and Bickle, 1988). In the Galápagos, there is a change in
20 lithospheric thickness from 70 km in the west to 40 km in the east (Villagómez et al.,
21 2007). As a result, western volcanoes undergo lower mean extents of melting than those
22 in the east (Gibson and Geist, 2010), despite a deeper onset of melting resulting from
23 higher excess temperatures (Villagómez et al., 2007) and chemical enrichment (White et
24 al., 1993). Mean extents of melting for magmas of a similar source composition can be
25 assessed from the ratios of REEs or slopes in primitive mantle normalized REE diagrams
26 (e.g., Gibson and Geist, 2010). At low extents of melting, light REEs will be fractionated
27 into the melt to greater extents than heavy REEs, creating relatively steep patterns and
28 elevated trace element ratios. The depth to the top of the melting column (serving as a
29 proxy for mean extent of melting) can be calculated from empirical relationships between
30 both $[La/Sm]_N$ and $[Sm/Yb]_N$, which are derived from REE inversion modeling (Eqs. 1, 2
31 in Gibson and Geist, 2010).

1 Determining relative extents of melting across the Galápagos is complicated by
2 mantle source heterogeneities, which also vary from west to east across the archipelago
3 (e.g., White et al., 1993). Lower negative slopes in REEs are predicted with increasing
4 distance from the plume due to decreasing extent of “plume” material in the source
5 (White et al., 1993). Fortunately, the degree of source enrichment can be evaluated
6 independently of melting processes through the use of radiogenic isotopes (e.g., Gibson
7 et al., 2012). While we have not measured radiogenic isotope ratios in the seamount
8 lavas, there is little variation in $^{87}\text{Sr}/^{86}\text{Sr}$ and $^{206}\text{Pb}/^{207}\text{Pb}$ in lavas with $[\text{La}/\text{Nb}]_{\text{N}} < 0.9$
9 from volcanoes adjacent to the seamounts (Wolf and Darwin; Western Santiago),
10 suggesting similar mantle sources (Gibson et al., 2012). Seamount lavas have $[\text{La}/\text{Nb}]_{\text{N}}$
11 ranging from 0.74–0.77, thus we assume a similar source composition between seamounts
12 and lavas erupted at nearby islands. Additionally, to minimize the impact of this
13 assumption, we choose to only evaluate depth to the top of the melting column using
14 $[\text{Sm}/\text{Yb}]_{\text{N}}$, which is less sensitive to source variation than $[\text{La}/\text{Sm}]_{\text{N}}$ (Gibson and Geist,
15 2010).

16 The mean REE slope of the western volcanoes is greater than that of the eastern
17 volcanoes, suggesting lower mean extents of melting, and consistent with a thicker
18 lithosphere (Fig. 7). The nearest western volcanoes to the seamounts (Wolf, Darwin and
19 Alcedo on Isabela Island) have mean $[\text{Sm}/\text{Yb}]_{\text{N}}$ of 2.55, attributed to a depth to the top of
20 the melting column at 57 km (Gibson and Geist, 2010). By comparison, eastern
21 volcanoes (Santiago and Santa Cruz Islands) have lower mean $[\text{Sm}/\text{Yb}]_{\text{N}}$ of 1.55, which
22 equates to a shallower depth to the top of the melting column of 53 km. Notably however,
23 there is a break in $[\text{Sm}/\text{Yb}]_{\text{N}}$ from W-E across the island of Santiago (56 km vs. 53 km,
24 respectively; Gibson et al., 2012) suggesting that the transition between thick and thin
25 lithosphere is relatively sharp and dissects the island into a western and eastern volcanic
26 system, assuming melts ascend vertically from their source. The seamount REE patterns
27 (Fig. 7) and ratios (Fig. 8) are intermediate between western and eastern volcanoes,
28 suggesting that magmas producing the seamounts were generated from intermediate
29 mean extents of melting. Seamount lavas have an average $[\text{Sm}/\text{Yb}]_{\text{N}}$ of 2.3 (Fig. 8),
30 corresponding to a depth to the top of the melting column of 56 km (Eq. 1 in Gibson and
31 Geist, 2010). This depth falls between that of the western and eastern volcanoes on

1 average, but is more consistent with the thicker lithosphere of the western volcanoes and
2 is identical to that of western Santiago.

3 4 *6.2. Crystallization and melt storage*

5 The seamounts are located within a major transition in volcano morphology and
6 magma storage depth between the western and eastern volcanic provinces on the
7 Galápagos Platform. Lavas erupted at western Galápagos volcanoes are produced by
8 relatively high extents of fractional crystallization (average MgO of 6.79 wt%; e.g., Saal
9 et al., 2007) in shallow crustal magma chambers (~200 MPa; Geist et al., 1998). By
10 contrast, lavas erupted at eastern volcanoes undergo less fractional crystallization
11 (average of 8.34 wt% MgO; Gibson et al., 2012; Wilson, 2013) at greater depths (~600
12 MPa; Geist et al., 1998).

13 All of the seamount lavas are relatively mafic, with MgO contents >7.7 wt. %,
14 suggesting limited crystallization prior to eruption. These MgO contents are higher than
15 the narrow range that is typically observed on the western islands of Fernandina and
16 Isabela (Fig. 3; e.g., Saal et al., 2007), but fall within the range of the eastern volcanoes
17 (Fig. 3; e.g., Gibson et al., 2012; Wilson, 2013). Petrologic modeling indicates that
18 crystallization depths of ~17-30 km (equivalent to 500-900 MPa; Fig. 4), consistent with
19 deeper magmatic plumbing systems at eastern volcanoes of ~21 km (Santa Cruz,
20 Santiago, San Cristobal; 600 +/- 100 MPa; Geist et al., 1998). Thus trace element patterns
21 and ratios of the seamount lavas share melting characteristics similar to western Santiago
22 and Wolf, Darwin and Alcedo volcanoes on Isabela, while the magma storage conditions
23 closely resemble those associated with the eastern volcanoes.

24 25 **7. Shared seamount magma plumbing with Santiago?**

26 The closest island to the two seamounts is Santiago (Fig. 2), which is 5 km to the
27 northeast, near the northern edge of the Galápagos Platform (Fig. 1). The island has
28 morphological characteristics of the eastern volcanoes, lacking a large central caldera and
29 having lower eruption rates compared to the more active western volcanoes (Fig. 1; Geist
30 et al., 2008b). Santiago remains volcanically active, with historical eruptions occurring
31 on the eastern side of the island in 1906 and on the western side in ~1754 (Siebert et al.,
32 2011). Lavas erupted on Santiago are highly variable, with rock types ranging from

1 picrites to trachytes (McBirney and Williams 1969; Saal et al., 2007; Herbert et al., 2009;
2 Gibson et al., 2012). Geochemical analyses of subaerial basalts indicate variable major
3 and trace element compositions (tholeiitic, transitional, and alkalic) that are spatially
4 distributed across the island (Gibson et al., 2012). The western portion of the island is
5 dominated by eruption of mildly alkaline basalts, while the eastern portion of the island
6 has erupted both tholeiitic and transitional basalts. This compositional zonation from west
7 to east is thought to occur due to an abrupt change in the lithospheric thickness directly
8 below Santiago (Gibson et al., 2012).

9 Trace element patterns in mildly alkaline lavas on western Santiago are
10 interpreted to result from melting directly beneath that side of the island, where thicker
11 lithosphere truncates the melting column at greater depths (Gibson et al., 2012). The
12 seamount lavas are compositionally similar to the mildly alkaline series and in particular,
13 a subset of lavas erupted subaerially on the western flank of Santiago (hereon referred to
14 as the Western Mildly Alkaline (WMA) lavas; Gibson et al., 2012). WMA lavas are
15 distinguished from other mildly alkalic lavas on the western side of the island by low
16 $[La/Ba]_N$ ratios and similar trace element patterns. Both the seamounts and WMA lavas
17 have undergone similar degrees of crystallization (means of 8.68 and 8.79 wt% MgO,
18 respectively) at similar storage depths of 17-35 km (interpreted from similar mean
19 CaO/Al_2O_3 of 0.67 and 0.65, respectively). Moreover, similar mantle source and degrees
20 of melting are inferred for seamount and WMA lavas based on REE abundances (10 and
21 11 mean ppm La, respectively) and mean $[La/Sm]_N$ ratios (1.38 and 1.51, respectively).
22 Similar depths to the top of the melting column are inferred from mean $[Sm/Yb]_N$ (2.26
23 and 2.35 respectively). The similarities between seamounts and WMA lavas are even
24 recognizable in the most nuanced variations in trace elements, including negative Ba
25 anomaly and slightly positive Sr and Zr anomalies (Fig. 9).

26 Based on these geochemical similarities, the seamount and WMA lavas are either
27 produced from a single magmatic event or two separate events, under nearly identical
28 conditions. If the seamounts were produced in a separate magmatic event, their chemical
29 similarities, outlined above, would require that they underwent the same degree of
30 melting of the same source, with similar transport and crystallization histories as the
31 WMA lavas. We assert that it is much simpler to assume that lavas for both seamounts
32 were produced in a single batch, and passed through the same magma plumbing system.

1 Thus, we conclude that the seamount and WMA lavas are sourced from the same central
2 reservoir in the lithospheric mantle (500-900 MPa; Fig. 10) beneath Santiago and erupted
3 over a relatively short time period. The distribution of WMA and seamount lavas implies
4 that, in the absence of shallow magma reservoirs in the eastern archipelago, magmas
5 stored deep in the crust can be transported laterally on the order of 10 km in subsurface
6 dikes prior to eruption (Fig. 10). We propose that lateral magma migration begins
7 between the transition into the elastic crust at 6-12 km (Feighner and Richards, 1994) and
8 depths derived from CO₂ and H₂O vapor saturation pressures at 1.2 km (Sec. 5; Fig. 10).
9 In Hawaii, similar dike dimensions (15-25 km lateral extent by 4-8 km vertical extent)
10 have been inferred from limits of seismic swarms during emplacement events (Rubin and
11 Pollard, 1988). This finding differs from that of Gibson et al. (2012), who, based on the
12 geochemistry of the subaerial sample suite suggest that there is limited lateral transport of
13 magmas during ascent through the lithosphere. This highlights the importance of
14 investigating submarine features around the main islands on the platform in order to
15 better understand the complexities of melt generation and construction of the archipelago.

16 Given the transitional nature and compositional similarity of the lavas from the
17 two seamounts and WMA lavas, in both maximum depths and extents of melting, we
18 prefer a model where melts may be generated in the mantle over a wide region between
19 Alcedo and Santiago (~50 km wide; Fig. 10), but are channeled through and
20 homogenized within the deep magmatic system associated with western Santiago prior to
21 their redistribution in the shallow crust. In this case, even if mantle heterogeneity or
22 lithospheric thickness undergo gradual changes across the archipelago, the variations are
23 discretized in the nearest island's complex plumbing system. Further geochemical and
24 morphological investigations of seamounts throughout the Galápagos Platform, and
25 comparisons to nearby volcanoes would help determine the extent to which the major
26 volcano magmatic systems control the geochemistry of intra-island seamounts.

27

28 **8. Conclusion**

29 Similarities in major and trace element concentrations and ratios suggest that
30 lavas erupted from two seamounts between the islands of Isabela and Santiago in the
31 Galápagos Archipelago are from the same parental magma. The seamounts were likely
32 produced by rapid magma ascent from depths >1.2 km, resulting in the construction of

1 the main edifices by both explosive and effusive volcanism. Magma supplied to the
2 seamounts were generated away from the plume center and underwent storage and minor
3 crystallization in a chamber located in the lithospheric mantle (17-35 km; Figs. 4, 10).

4 Total extents of melting, as indicated by intermediate average REE patterns, and
5 $[\text{Sm}/\text{Yb}]_N$ are transitional between the western and eastern regions of the archipelago
6 (Figs. 7, 8; Gibson and Geist, 2010), and closely resemble those of the nearby western
7 volcanoes of Wolf, Darwin and Alcedo on Isabela Island, as well as western Santiago, in
8 average trace element contents (Fig. 5). These data suggest that seamount magmas were
9 generated above a lithosphere of intermediate thickness similar conditions beneath
10 eastern Isabela and western Santiago. Despite this, seamount magmas appear to have a
11 transport and storage history more akin to that of the eastern volcanoes (e.g., low extents
12 of fractional crystallization, Fig. 3; deep storage, Fig. 4), reflecting lower magma supply
13 and deeper crystallization. These compositional characteristics signify that, although
14 seamount magmas have a transitional melting signature, their crustal signature suggests
15 they are parasitic to Santiago and pass through a shared plumbing system that has also
16 erupted subaerial lavas (Fig. 10).

17 Given the transitional nature of the seamount lavas, in both maximum depths and
18 extents of melting, between that of the western and eastern volcanoes, we prefer a model
19 where melts are generated over a ~50 km wide region beneath the seamounts and the
20 island, but are homogenized in the lithospheric mantle and are channeled through western
21 Santiago's crustal plumbing system and transported laterally on the order of 10 km in
22 subsurface dikes prior to eruption on the shallow submarine platform (Fig. 10). The
23 Galápagos Platform is studded with numerous clusters and lineaments of small
24 seamounts adjacent to the islands, most of which have never been sampled. Further
25 detailed geological and geochemical investigations of these seamounts and their
26 relationship to adjacent volcanoes would enable a better assessment of the extent of
27 magma partitioning between subaerial and submarine systems' relationship to seamount
28 and subaerial morphologies as well as the origins of the magmas in both settings.

30 **Acknowledgements**

31 We thank the Ocean Exploration Trust, and the crew of the *E/V Nautilus* for facilitating
32 the mapping and sample collection for this project. Thank you to the NOAA Office of

1 Exploration and Research for funding the E/V *Nautilus* Exploration Program
2 (NA15OAR0110220). Additionally, we are grateful to the Galápagos National Park
3 directorate for allowing the collection of submarine rock samples through joint permit
4 (PC-45-15) in collaboration with the Charles Darwin Research Foundation. We
5 appreciate the WSU Geoanalytical Facility and WHOI Ionprobe Facility for XRF and
6 volatile analysis, respectively. Work for this project was carried out with support
7 provided by the NSF (OCE-1634952) to VDW and the Dalio Explore Fund at WHOI.

8

9 **References**

- 10 Allan, J.F., Simkin, T., 2000. Fernandina Volcano's evolved, well-mixed basalts:
11 Mineralogical and petrological constraints on the nature of the Galápagos plume.
12 *J. Geophys. Res.* 105, 6017. doi:10.1029/1999JB900417
- 13 Allen, S.R., McPhie, J., 2009. Products of neptunian eruptions. *Geology* 37, 639–642.
- 14 Asimow, P.D., Ghiorso, M.S., 1998. Algorithmic modifications extending MELTS to
15 calculate subsolidus phase relations. *Am. Mineral.* 83, 1127–1132.
- 16 Bell, K.L.C., Brennan, M.L., Flanders, J., Raineault, N.A., Wagner, K., 2016. New
17 Frontiers in Ocean Exploration: The E/V *Nautilus* and NOAA Ship *Okeanos*
18 Explorer, 2015 Field Season.
- 19 Carey, B.S., Fisher, C.R., Leon, P.S. De, Roman, C., Raineault, N.A., Suarez, J., Smart,
20 C., Kane, R., Tüzün, S., Balcanoff, J., Lubetkin, M., Jones, M., Schwartz, D.,
21 Fornari, D., Soule, A., Wanless, D., Watling, L., Ballard, R.D., 2016. Exploring
22 the Undersea World of the Galápagos Islands Exploring the Undersea World of
23 the Galápagos Islands.
- 24 Chadwick, W.W., Dieterich, J.H., 1995. Mechanical modeling of circumferential and
25 radial dike intrusion on Galápagos volcanoes. *J. Volcanol. Geotherm. Res.* 66,
26 37–52.
- 27 Chadwick, W.W., Howard, K.A., 1991. The pattern of circumferential and radial eruptive
28 fissures on the volcanoes of Fernandina and Isabela islands, Galápagos. *Bull.*
29 *Volcanol.* 53, 259–275. doi:10.1007/BF00414523
- 30 Christie, D.M., Duncan, R.A., McBirney, A.R., Richards, M.A., White, W.M., Harpp,
31 K.S., Fox, C.G., 1992. Drowned islands downstream from the Galápagos hotspot
32 imply extended speciation times. *Nature* 355, 246–248. doi:10.1038/355246a0
- 33 Clague, D.A., Dalrymple, G.B., 1987. The Hawaiian-Emperor volcanic chain. Part I.
34 Geologic evolution. *Volcanism in Hawaii* 1, 5–54.
- 35 Dixon, J.E., Stolper, E.M., 1995. An experimental study of water and carbon dioxide
36 solubilities in mid-ocean ridge basaltic liquids. Part II: applications to degassing.
37 *J. Petrol.* 36, 1633–1646.
- 38 Dixon, J.E., Stolper, E.M., Delaney, J.R., 1988. Infrared spectroscopic measurements of
39 CO₂ and H₂O in Juan de Fuca Ridge basaltic glasses. *Earth Planet. Sci. Lett.* 90,
40 87–104. doi:10.1016/0012-821X(88)90114-8
- 41 Feighner, M.A., Richards, M.A., 1994. Lithospheric structure and compensation
42 mechanisms of the Galápagos Archipelago. *J. Geophys. Res.* 99, 6711–6729.

- 1 Geist, D., 1996. On the emergence and submergence of the Galápagos Islands. *Not.*
2 *Galápagos* 56, 5–9.
- 3 Geist, D., Diefenbach, B. a., Fornari, D.J., Kurz, M.D., Harpp, K., Blusztajn, J., 2008a.
4 Construction of the Galápagos platform by large submarine volcanic terraces.
5 *Geochemistry, Geophys. Geosystems* 9. doi:10.1029/2007GC001795
- 6 Geist, D.J., Harpp, K.S., Naumann, T.R., Poland, M., Chadwick, W.W., Hall, M., Rader,
7 E., 2008b. The 2005 eruption of Sierra Negra volcano, Galápagos, Ecuador. *Bull.*
8 *Volcanol.* 70, 655–673. doi:10.1007/s00445-007-0160-3
- 9 Geist, D., Harpp, K., 2009. Galápagos Islands: Geology. *Encycl. Islands.*
- 10 Geist, D.J., McBirney, A.R., Duncan, R. a., 1986. Geology and petrogenesis of lavas
11 from San Cristobal Island, Galapagos Archipelago. *Geol. Soc. Am. Bull.* 97, 555.
12 doi:10.1130/0016-7606(1986)97<555:GAPOLF>2.0.CO;2
- 13 Geist, D., Naumann, T., Larson, P., 1998. Evolution of Galápagos magmas: Mantle and
14 crustal fractionation without assimilation. *J. Petrol.* 39, 953–971.
- 15 Geist, D., Snell, H., Snell, H., Goddard, C., Kurz, M.D., 2014a. A paleogeographic model
16 of the Galápagos Islands and biogeographical and evolutionary implications, in:
17 Karen S. Harpp, Eric Mittelstaedt, Noémi d’Ozouville, and D.W.G. (Ed.), *The*
18 *Galápagos: A Natural Laboratory for the Earth Sciences*, Geophysical Monograph
19 204. John Wiley & Sons, Inc., pp. 145–166.
- 20 Geist, D.J., Bergantz, G., Chadwick, W.W., 2014b. Galápagos Magma Chambers, in:
21 Karen S. Harpp, Eric Mittelstaedt, Noémi d’Ozouville, and D.W.G. (Ed.), *The*
22 *Galápagos: A Natural Laboratory for the Earth Sciences*, Geophysical Monograph
23 204. John Wiley & Sons, Inc., pp. 55–70.
- 24 Ghiorsso, M.S., Sack, R.O., 1995. Chemical mass transfer in magmatic processes IV. A
25 revised and internally consistent thermodynamic model for the interpolation and
26 extrapolation of liquid-solid equilibria in magmatic systems at elevated
27 temperatures and pressures. *Contrib. to Mineral. Petrol.* 119, 197–212.
- 28 Gibson, S., Geist, D., 2010. Geochemical and geophysical estimates of lithospheric
29 thickness variation beneath Galápagos. *Earth Planet. Sci. Lett.* 300, 275–286.
30 doi:10.1016/j.epsl.2010.10.002
- 31 Gibson, S., Geist, D.J., Day, J. a., Dale, C.W., 2012. Short wavelength heterogeneity in
32 the Galápagos plume: Evidence from compositionally diverse basalts on Isla
33 Santiago. *Geochemistry Geophys. Geosystems* 13, Q09007.
34 doi:10.1029/2012GC004244
- 35 Goss, A.R., Perfit, M.R., Ridley, W.I., Rubin, K.H., Kamenov, G.D., Soule, S.A., Fundis,
36 A., Fornari, D.J., 2010. Geochemistry of lavas from the 2005-2006 eruption at the
37 East Pacific Rise, 9°46’N-9°56’N: Implications for ridge crest plumbing and
38 decadal changes in magma chamber compositions. *Geochemistry, Geophys.*
39 *Geosystems* 11, 1–35. doi:10.1029/2009GC002977
- 40 Harpp, K., Geist, D., 2002. Wolf–Darwin lineament and plume–ridge interaction in
41 northern Galápagos. *Geochemistry, Geophys. Geosystems* 3, 1–19.
- 42 Harpp, K.S., Fornari, D.J., Geist, D.J., Kurz, M.D., 2003. Genovesa Submarine Ridge: A
43 manifestation of plume - ridge interaction in the northern Galápagos Islands.
44 *Geochemistry, Geophys. Geosystems* 4.
- 45 Hauri, E., Wang, J., Dixon, J.E., King, P.L., Mandeville, C., Newman, S., 2002. SIMS
46 analysis of volatiles in silicate glasses 1. Calibration, matrix effects and

1 comparisons with FTIR. *Chem. Geol.* 183, 99–114. doi:10.1016/S0009-
2 2541(01)00375-8

3 Herbert, S., Gibson, S., Norman, D., Geist, D.J., Estes, G., Grant, T., Miles, A., 2009.
4 Into the field again: re-examining Charles Darwin's 1835 geological work on Isla
5 Santiago (James Island) in the Galápagos Archipelago. *Earth Sci. Hist.*

6 Hooft, E.E.E., Toomey, D.R., Solomon, S.C., 2003. Anomalously thin transition zone
7 beneath the Galápagos hotspot. *Earth Planet. Sci. Lett.* 216, 55–64.

8 Jackson, M.G., Hart, S.R., Saal, A.E., Shimizu, N., Kurz, M.D., Blusztajn, J.S.,
9 Skovgaard, A.C., 2008. Globally elevated titanium, tantalum, and niobium
10 (TITAN) in ocean island basalts with high $^3\text{He}/^4\text{He}$. *Geochemistry, Geophys.*
11 *Geosystems* 9. doi:10.1029/2007GC001876

12 Johnson, D.M., Hooper, P.R., Conrey, R.M., 1999. XRF analysis of rocks and minerals
13 for major and trace elements on a single low dilution Li-tetraborate fused bead.
14 *Adv. X-ray Anal.* 41, 843–867.

15 Kelley, K.A., Plank, T., Ludden, J., Staudigel, H., 2003. Composition of altered oceanic
16 crust at ODP Sites 801 and 1149. *Geochemistry, Geophys. Geosystems* 4.

17 Koleszar, A.M., Saal, A.E., Hauri, E.H., Nagle, A.N., Liang, Y., Kurz, M.D., 2009. The
18 volatile contents of the Galápagos plume; evidence for H₂O and F open system
19 behavior in melt inclusions. *Earth Planet. Sci. Lett.* 287, 442–452.

20 Kurz, M., Geist, D., 1999. Dynamics of the Galápagos hotspot from helium isotope
21 geochemistry. *Geochim. Cosmochim. Acta* 63, 4139–4156.

22 Kurz, M.D., Curtice, J., Fornari, D., Geist, D., Moreira, M., 2009. Primitive neon from
23 the center of the Galápagos hotspot. *Earth Planet. Sci. Lett.* 286, 23–34.
24 doi:10.1016/j.epsl.2009.06.008

25 le Roux, P.J., Shirey, S.B., Hauri, E.H., Perfit, M.R., Bender, J.F., 2006. The effects of
26 variable sources, processes and contaminants on the composition of northern EPR
27 MORB (8–10 N and 12–14 N): Evidence from volatiles (H₂O, CO₂, S) and
28 halogens (F, Cl). *Earth Planet. Sci. Lett.* 251, 209–231.

29 Lytle, M.L., Kelley, K.A., Hauri, E.H., Gill, J.B., Papia, D., Arculus, R.J., 2012. Tracing
30 mantle sources and Samoan influence in the northwestern Lau back-arc basin.
31 *Geochemistry, Geophys. Geosystems* 13.

32 McBirney, A.R., Williams, H., 1969. Geology and petrology of the Galápagos Islands.
33 *Geol. Soc. Am. Mem.* 118, 1–197.

34 McDonough, W.F., Sun, S.S., 1995. The composition of the Earth. *Chem. Geol.* 120,
35 223–253.

36 McKenzie, D., Bickle, M.J., 1988. The volume and composition of melt generated by
37 extension of the lithosphere. *J. Petrol.* 29, 625–679.

38 Morgan, W.J., 1972. Deep mantle convection plumes and plate motions. *Am. Assoc. Pet.*
39 *Geol. Bull.* 56, 203–213.

40 Newman, S., Lowenstern, J.B., 2002. VolatileCalc: a silicate melt–H₂O–CO₂ solution
41 model written in Visual Basic for Excel. *Comput. Geosci.* 28, 597–604.

42 Peterson, M., Saal, A.E., Hauri, E.H., Werner, R., Hauff, S.F., Kurz, M.D., Geist, D.,
43 Harpp, K.S., 2010. Sources of volatiles in basalts from the Galápagos
44 Archipelago: deep and shallow evidence, in: AGU Fall Meeting Abstracts.

45 Peterson, M., Saal, A., Hauri, E., Kurz, M., Werner, R., Hauff, F., Geist, D., Harpp, K.,
46 2013. Volatile Budget of the Galápagos Plume. *Goldschmidt 2013 Conf. Abstr.*
47 1956.

- 1 Rilling, S.E., 2005. Oxygen Fugacities of Lavas from the Galápagos Islands and the
2 Galápagos Spreading Center, in: AGU Fall Meeting Abstracts.
- 3 Rowland, S.K., 1996. Slopes, lava flow volumes, and vent distributions on Volcan
4 Fernandina, Galápagos Islands. *J. Geophys. Res. Solid Earth* 101, 27657–27672.
- 5 Rubin, A.M., Pollard, D.D., 1988. Dike-induced faulting in rift zones of Iceland and
6 Afar. *Geology* 16, 413–417.
- 7 Saal, A.E., Hauri, E.H., Langmuir, C.H., Perfit, M.R., 2002. Vapour undersaturation in
8 primitive mid-ocean-ridge basalt and the volatile content of Earth's upper mantle
9 41.
- 10 Saal, A.E., Kurz, M.D., Hart, S.R., Blusztajn, J.S., Blichert-Toft, J., Liang, Y., Geist,
11 D.J., 2007. The role of lithospheric gabbros on the composition of Galápagos
12 lavas. *Earth Planet. Sci. Lett.* 257, 391–406.
- 13 Settle, M., 1979. The structure and emplacement of cinder cone fields. *Am. J. Sci.* 279,
14 1089–1107.
- 15 Shaw, D.M., 1970. Trace element fractionation during anatexis. *Geochim. Cosmochim.*
16 *Acta* 34, 237–243.
- 17 Siebert, L., Simkin, T., Kimberly, P., 2011. *Volcanoes of the World*. Univ of California
18 Press.
- 19 Simkin, T., Howard, K.A., 1970. Caldera collapse in the Galápagos Islands, 1968.
20 *Science* (80). 169, 429–437.
- 21 Simkin, T., Siebert, L., 1994. *Volcanoes of the World: A Regional Directory, Gazetteer,*
22 *and Chronology of Volcanism During the Last 10,000 Years*, 349 pp. Geosci.
23 Press. Tucson, Ariz.
- 24 Smith, P.M., Asimow, P.D., 2005. Adibat_1ph: A new public front-end to the MELTS,
25 pMELTS, and pHMELTS models. *Geochemistry, Geophys. Geosystems* 6.
- 26 Swanson, F.J., Baitis, H.W., Lexa, J., Dymond, J., 1974. Geology of Santiago, Rábida,
27 and Pinzón Islands, Galápagos. *Geol. Soc. Am. Bull.* 85, 1803–1810.
- 28 Toomey, D.R., Hooft Toomey, E.E., Hooft Toomey, E.E., Detrick, R.S., 2001. Crustal
29 thickness variations and internal structure of the Galápagos Archipelago, in: AGU
30 Fall Meeting Abstracts.
- 31 Villagómez, D.R., Toomey, D.R., Hooft, E.E.E., Solomon, S.C., 2011. Crustal structure
32 beneath the Galpagos Archipelago from ambient noise tomography and its
33 implications for plume-lithosphere interactions. *J. Geophys. Res. Solid Earth* 116,
34 1–20. doi:10.1029/2010JB007764
- 35 Villagómez, D.R., Toomey, D.R., Hooft, E.E.E., Solomon, S.C., 2007. Upper mantle
36 structure beneath the Galápagos Archipelago from surface wave tomography. *J.*
37 *Geophys. Res.* 112, B07303. doi:10.1029/2006JB004672
- 38 Weaver, B.L., 1991. The origin of ocean island basalt end-member compositions: trace
39 element and isotopic constraints. *Earth Planet. Sci. Lett.* 104, 381–397.
- 40 White, W.M., McBirney, A.R., Duncan, R.A., 1993. Petrology and geochemistry of the
41 Galápagos Islands: Portrait of a pathological mantle plume. *J. Geophys. Res.*
42 *Solid Earth* 98, 19533–19563.
- 43 Wilson, E.L., 2013. *The geochemical evolution of Santa Cruz Island, Galápagos*
44 *Archipelago*. University of Idaho.
- 45 Yun, S., Segall, P., Zebker, H., 2006. Constraints on magma chamber geometry at Sierra
46 Negra Volcano, Galápagos Islands, based on InSAR observations. *J. Volcanol.*
47 *Geotherm. Res.* 150, 232–243. doi:10.1016/j.jvolgeores.2005.07.009

Sample Locations

sample	long	lat	elev (m)
Northern Seamount			
NA064-114	-90.81503	-0.37395	-422
NA064-115	-90.81612	-0.37255	-439
NA064-116	-90.81627	-0.37220	-420
NA064-120	-90.81763	-0.37630	-450
NA064-123	-90.81772	-0.37668	-445
NA064-127	-90.81770	-0.37840	-469
Southern Seamount			
NA064-129	-90.81792	-0.38047	-472
NA064-131	-90.81907	-0.40192	-265
NA064-132	-90.81797	-0.40003	-329
NA064-133	-90.81900	-0.40025	-325
NA064-134	-90.83197	-0.39960	-588
NA064-135	-90.83233	-0.39998	-587

Table 1: Sample names and locations.

1

XRF Derived Major/Trace Element Concentrations and SIMS Derived Volatile Element Concentrations

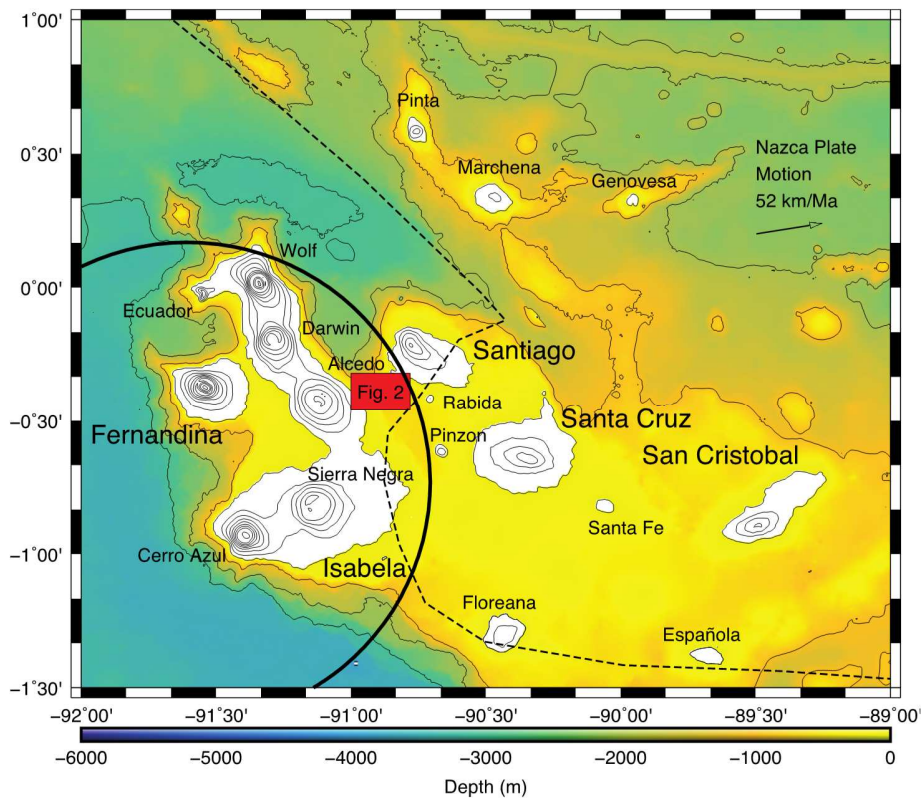
NA064													
-	114	115	116	120	123	127	129	131	132	133	134	135	
Major Element Concentrations (wt%)													
SiO2	44.64	44.44	44.26	46.72	46.24	46.54	45.27	46.61	46.48	46.33	45.07	46.65	46.80
TiO2	2.238	2.178	2.167	2.248	2.324	2.380	2.386	2.318	2.253	2.368	2.372	2.438	2.342
Al2O3	15.31	15.18	15.16	16.07	15.76	15.89	15.68	16.03	15.56	15.76	15.80	15.73	15.71
FeO*	11.52	14.42	14.27	11.69	12.06	12.45	12.85	12.21	11.35	11.51	11.69	11.81	11.66
MnO	0.175	0.190	0.188	0.191	0.209	0.185	0.190	0.212	0.176	0.177	0.161	0.185	0.180
MgO	8.64	8.36	8.34	8.10	8.88	8.17	8.36	8.99	9.42	8.87	7.74	8.77	8.70
CaO	11.95	9.10	9.06	10.81	10.20	10.34	10.10	10.08	10.59	10.53	11.49	10.23	10.35
Na2O	2.78	2.52	2.52	2.85	2.88	2.90	2.82	2.84	2.75	2.93	2.66	2.96	2.85
K2O	0.39	0.61	0.61	0.37	0.38	0.42	0.42	0.39	0.36	0.34	0.40	0.38	0.46
P2O5	0.257	0.489	0.485	0.277	0.283	0.282	0.326	0.266	0.247	0.254	0.775	0.258	0.258
Sum	97.90	97.48	97.06	99.32	99.21	99.56	98.40	99.95	99.18	99.07	98.16	99.41	99.30
LOI %	1.74	2.16	2.16	0.00	0.00	0.00	0.76	0.00	0.00	0.00	1.38	0.00	0.00
Trace Element Concentrations (ppm)													
Ni	173	176	178	142	178	158	163	179	192	168	182	163	162
Cr	239	282	282	244	246	229	247	247	334	284	358	231	276
Sc	27	28	27	31	30	29	27	29	30	30	31	28	29
V	250	249	245	277	268	283	267	265	275	279	282	278	275
Ba	66	65	70	65	72	72	72	75	68	70	62	74	68
Rb	7	11	10	5	7	7	7	7	6	5	8	7	8
Sr	717	352	350	311	319	315	387	313	318	327	400	335	323
Zr	147	144	143	148	151	155	157	152	146	152	148	154	154
Y	27	27	26	28	28	30	29	28	27	27	31	28	27
Nb	12.5	11.1	11.4	12.3	12.5	13.3	12.4	13.0	12.1	13.3	12.9	13.6	12.3
Ga	19	17	16	20	19	19	19	20	19	19	18	20	20
Cu	61	55	57	71	61	54	60	59	68	67	51	66	66
Zn	97	108	114	101	108	108	110	114	104	184	175	134	114
Pb	1	1	1	2	1	1	2	1	1	1	3	1	1
La	12	9	10	11	9	13	16	15	12	10	14	12	12
Ce	29	25	24	30	29	30	30	27	25	32	26	33	28
Th	2	2	1	1	1	1	2	1	0	1	2	2	1
Nd	18	16	17	20	20	19	18	19	19	20	20	20	19
U	2	9	7	1	2	2	2	1	1	2	4	1	3
Volatile Element Concentrations (ppm)													
NA064													
-	H2O	CO2	S	Cl	F								
114	8700	135	1636	210	891								

Table 2: XRF derived major and trace element concentrations for seamount lavas, and SIMS derived volatile concentrations for sample NA064-114. Analytical precision is reported in Johnson et al., (1999).

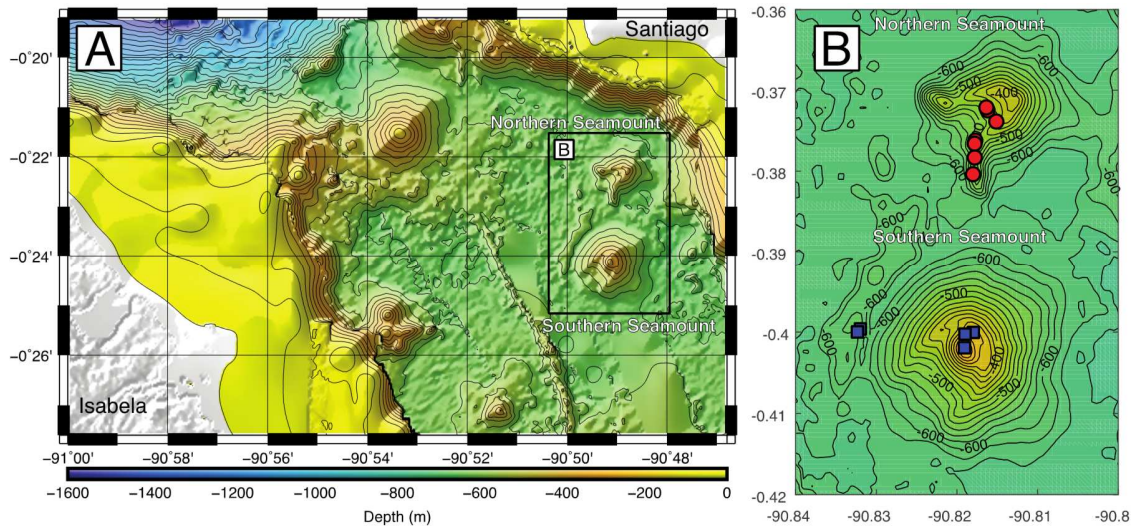
ICPMS Derived Trace Element Concentrations

NA-064-	114	115	116	120	123	127	129	131	132	133	134	135
Li	6.11	5.51	5.39	5.57	5.83	6.06	5.48	6.67	6.28	5.54	5.89	5.15
Sc	27.9	27.8	31.5	27.6	29.1	28.0	26.7	32.1	29.0	29.9	26.3	28.7
V	240	238	264	243	253	244	232	278	255	256	239	245
Cr	235	184	184	201	184	196	188	270	220	287	218	219
Co	57.6	48.2	48.3	56.6	49.5	51.3	56.8	48.1	52.5	51.3	51.0	52.0
Ni	200	139	113	189	126	149	217	124	165	196	153	167
Cu	76.6	63.8	73.2	78.6	59.8	62.5	57.9	83.9	72.5	65.8	62.0	64.5
Zn	117.0	120.3	123.2	110.8	112.6	114.0	110.0	114.8	295.1	114.6	110.9	107.4
Ga	12.9	12.5	13.4	12.6	13.4	13.0	12.7	13.3	13.3	12.8	13.5	12.9
Rb	6.53	6.03	6.32	6.03	6.52	6.42	6.06	6.25	5.49	8.20	5.23	6.76
Sr	312	296	306	301	317	308	303	337	319	342	344	314
Y	27.4	26.1	29.1	27.1	28.5	27.8	26.2	29.5	27.8	28.1	26.3	26.6
Zr	167	147	151	146	155	156	145	170	159	155	150	151
Nb	14.3	12.6	13.8	13.8	14.4	14.1	13.4	14.7	14.7	13.7	14.5	14.2
Cs	0.06	0.07	0.06	0.06	0.07	0.06	0.06	0.06	0.05	0.22	0.05	0.07
Ba	60.2	56.5	60.2	60.1	63.1	63.3	58.8	63.9	65.0	56.3	64.0	60.9
La	10.5	9.4	10.3	10.2	10.6	10.5	9.9	11.0	10.9	10.2	11.0	10.5
Ce	27.1	24.4	26.8	26.4	27.6	27.4	25.1	28.2	27.9	26.3	27.9	26.7
Pr	3.94	3.58	3.93	3.86	4.07	3.96	3.69	4.19	4.15	3.93	4.11	3.85
Nd	17.8	16.2	17.9	17.5	18.5	18.1	16.8	19.3	18.9	17.9	18.7	18.2
Sm	4.65	4.34	4.77	4.63	4.87	4.78	4.46	5.06	4.83	4.65	4.86	4.68
Eu	1.62	1.50	1.65	1.58	1.66	1.65	1.54	1.74	1.72	1.63	1.67	1.62
Gd	5.33	4.98	5.54	5.29	5.64	5.55	5.11	5.74	5.56	5.38	5.44	5.28
Tb	0.92	0.85	0.94	0.90	0.96	0.92	0.87	0.97	0.92	0.91	0.90	0.89
Dy	5.19	4.84	5.37	5.10	5.29	5.26	4.76	5.54	5.10	5.13	5.02	4.97
Ho	0.99	0.95	1.05	0.98	1.01	1.02	0.94	1.08	1.01	1.02	0.98	0.99
Er	2.60	2.52	2.79	2.53	2.69	2.65	2.45	2.82	2.65	2.64	2.52	2.53
Tm	0.38	0.37	0.42	0.38	0.40	0.39	0.36	0.42	0.39	0.39	0.36	0.37
Yb	2.28	2.17	2.45	2.23	2.31	2.32	2.13	2.44	2.25	2.31	2.16	2.15
Lu	0.34	0.32	0.37	0.33	0.34	0.34	0.32	0.36	0.33	0.34	0.31	0.32
Hf	3.91	3.63	3.99	3.86	4.04	4.01	3.73	4.11	4.05	3.91	3.95	3.91
Ta	1.04	0.84	0.92	0.92	0.96	0.96	0.87	0.94	0.96	0.91	0.97	0.93
Pb	1.87	0.86	0.97	1.06	1.21	0.78	0.71	2.63	1.17	1.09	1.22	0.91
Th	0.89	0.76	0.83	0.84	0.88	0.86	0.80	0.86	0.87	0.80	0.92	0.84
U	0.31	0.61	0.47	0.71	0.80	0.32	0.33	0.33	0.29	1.74	0.28	0.57

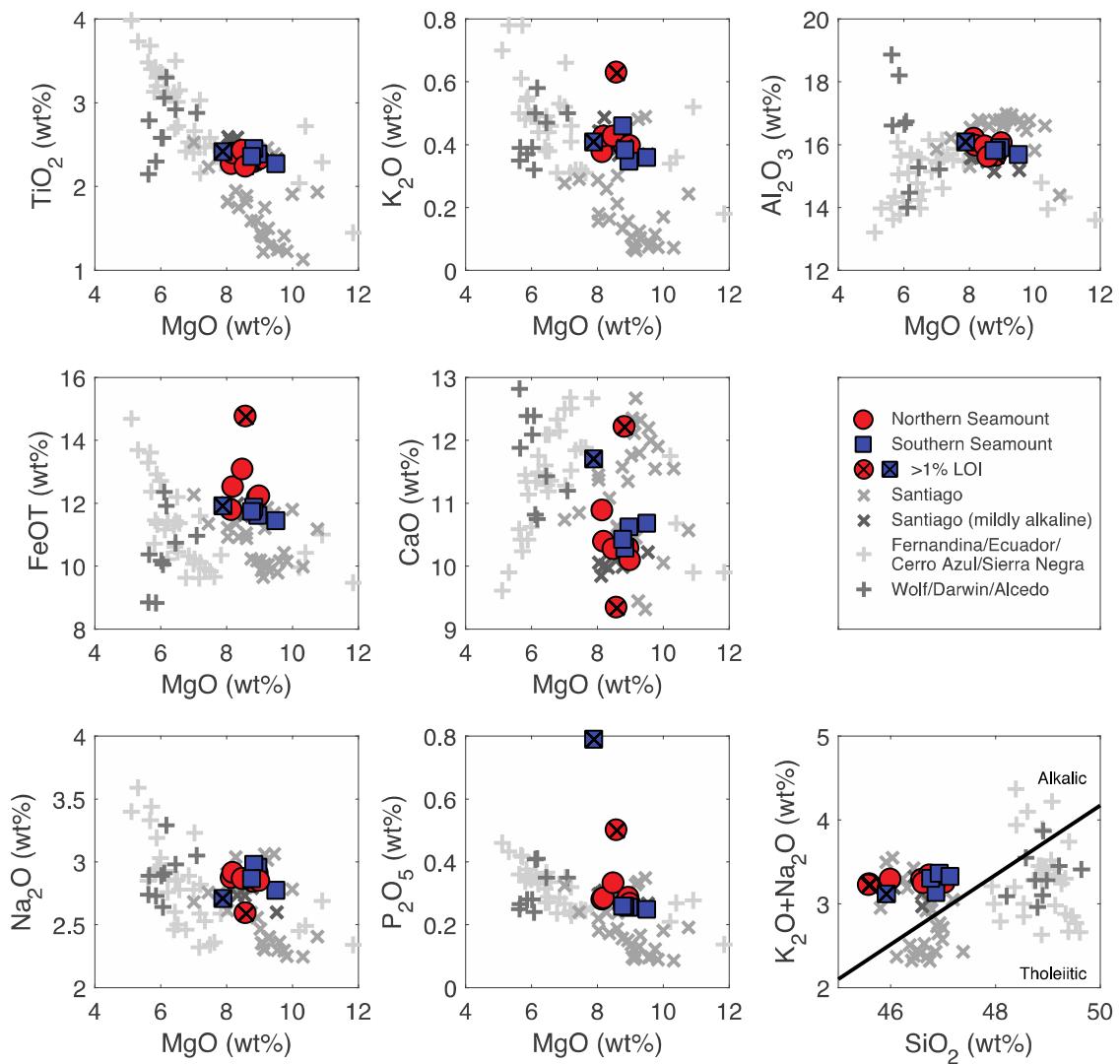
Table 3: ICPMS derived trace element contents for seamount lavas; all concentrations are reported in ppm. Analytical precision is reported in the supplementary data tables.



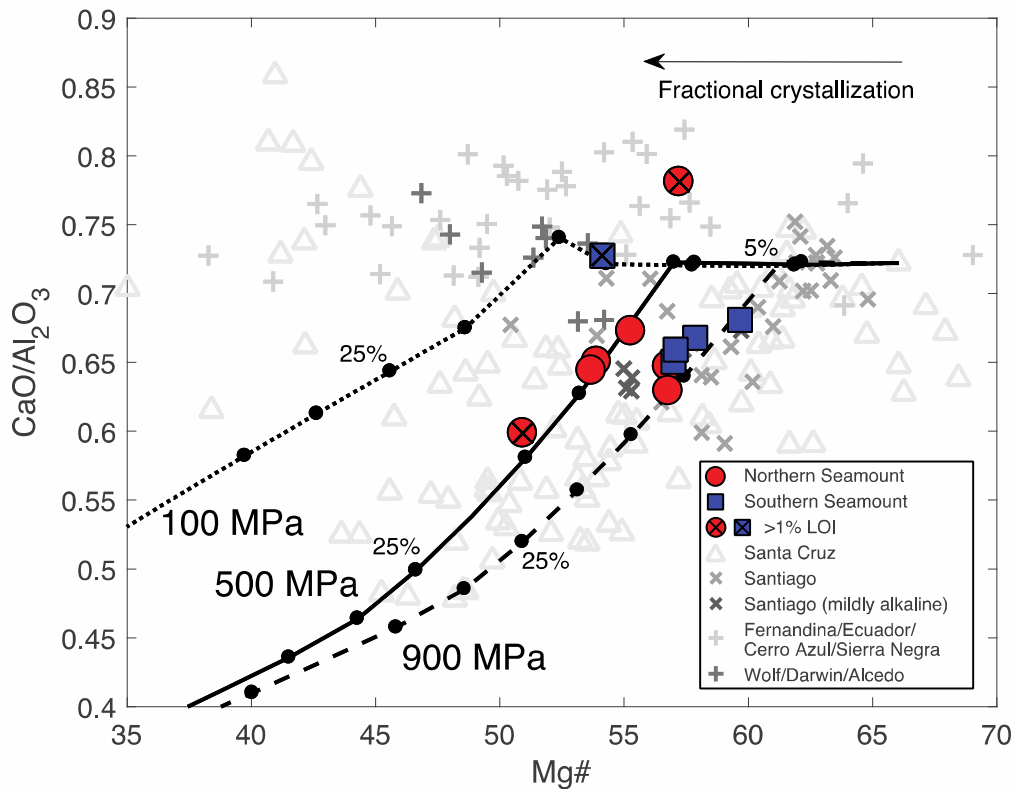
1
2 **Fig. 1: Map of the Galápagos Archipelago** The western islands (Isabela, Fernandina)
3 are typified by steep upper flanks and central calderas, eastern islands (Santiago, Santa
4 Cruz, San Cristobal) have shallow slopes and are characterized by dispersed linear
5 volcanic vent systems. Subaerial contours show elevations at 200 m intervals. Submarine
6 contours show bathymetry at 500 m intervals. Solid black circle indicates boundary of
7 anomalously thin mantle transition zone, inferred as plume upwelling region centered
8 below Fernandina (Hooft et al., 2003). Dashed line shows boundary between high (12 km
9 to the west) and low (6 km to the east) effective elastic thickness of the crust (Feighner
10 and Richards, 1994), which correlates with the boundary of thick and thin mantle
11 lithosphere (Villagómez et al., 2007). Location of seamounts sampled in this study is
12 shown by the red region, and in more detail in Fig. 2.
13



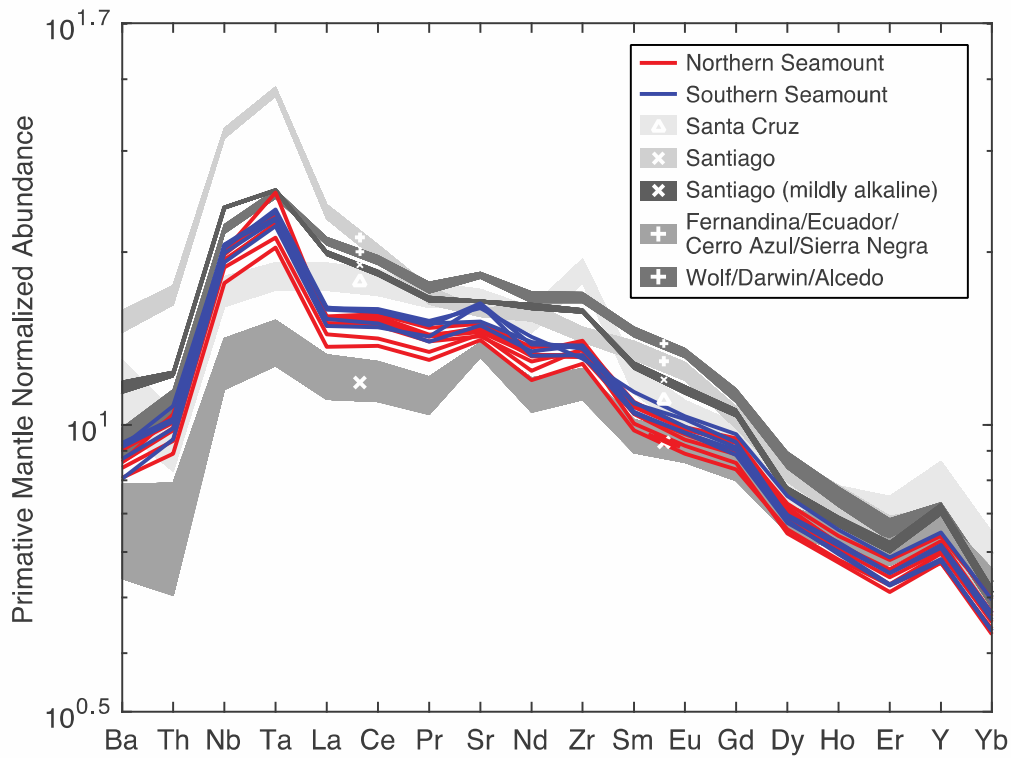
1
 2 **Fig. 2: A) Bathymetric Map of the Northern and Southern Seamount Region** The
 3 seamounts are in the central Galápagos and are on top of the Galápagos platform with
 4 basal depths ~600 m. Contour interval is 50 m. The nearest islands are Santiago, 5 km to
 5 the northeast, and Isabela, 10 km to the west. Black box shows location of inset map. **B)**
 6 **Inset Map of Seamounts** Colored symbols show sample locations. Colormap is the same
 7 as in A, contour interval is 20 m.



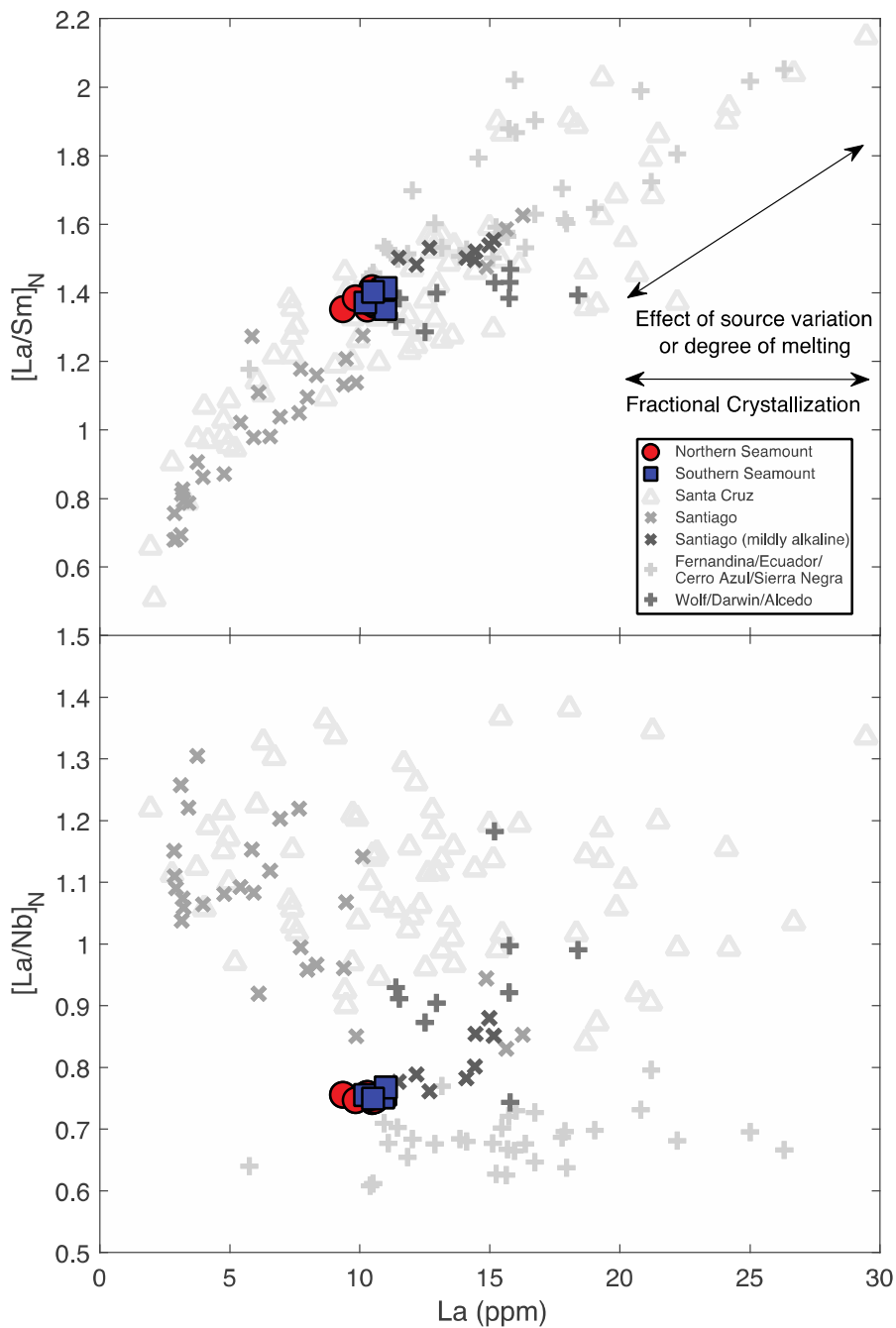
1
2 **Fig. 3: Major Element Variations of Seamount Lavas** Outlined colored markers show
3 data from this study. Samples with loss on ignition (LOI) >1 wt% are indicated with
4 black “X”. Grey markers show representative lavas from nearby Galápagos volcanoes
5 (Fernandina, Ecuador, Cerro Azul, Sierra Negra, Wolf, Darwin, Alcedo; Saal et al., 2007;
6 Santiago; Gibson et al., 2012). Where not visible, dark grey exes indicating the mildly
7 alkaline Santiago compositions are plotted directly beneath seamount data points.
8



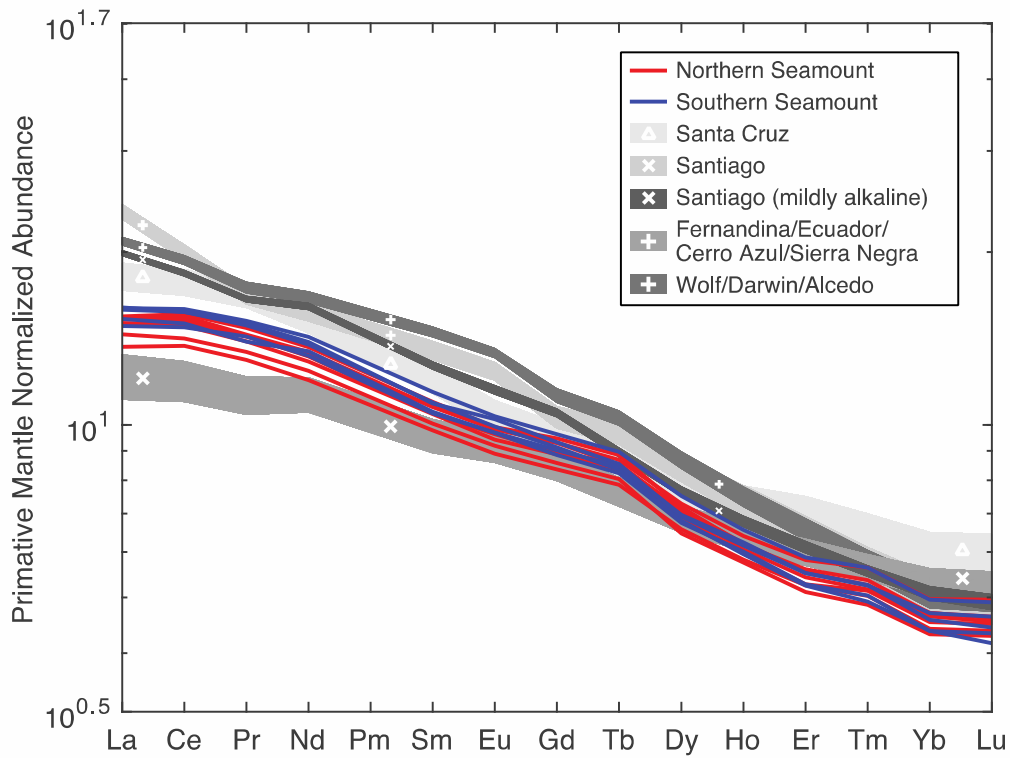
1
2 **Fig. 4: Variation of $\text{CaO}/\text{Al}_2\text{O}_3$ as a Function of Mg#** Mg# is defined as molecular
3 $\text{MgO}/(\text{MgO}+\text{FeO}_T)*100$. Black lines show isobaric fractional crystallization trends at
4 100, 500 and 900 MPa, black dots along lines indicate 5% increments of crystal
5 fractionation by mass. Fractional crystallization is modeled from alphaMELTS software
6 (see text for model descriptions). Outlined colored markers show data from this study.
7 Samples with loss on ignition (LOI) >1 wt% are indicated with black “X”. Grey markers
8 show representative lavas from nearby Galápagos volcanoes (Fernandina, Ecuador, Cerro
9 Azul, Sierra Negra, Wolf, Darwin, Alcedo; Saal et al., 2007; Santiago; Gibson et al.,
10 2012; Santa Cruz; Wilson, 2013).



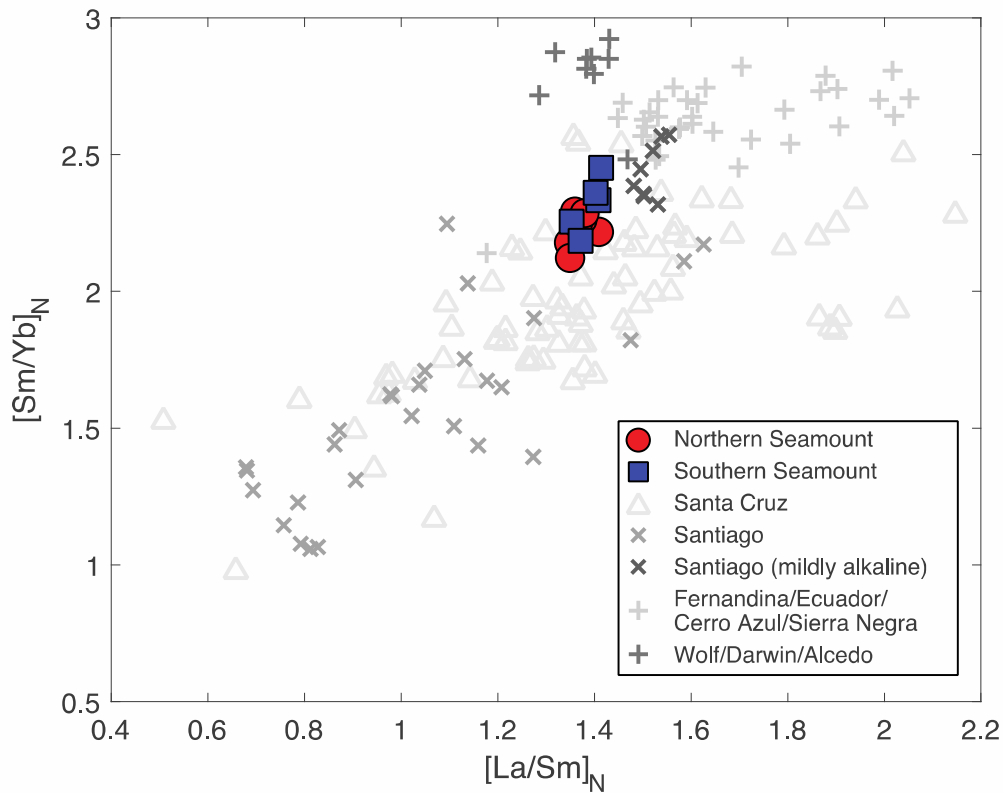
1
 2 **Fig. 5: Trace Element Diagram Comparing the Seamount Samples to Averaged**
 3 **Galápagos Lavas** Elements are listed in order of increasing compatibility and
 4 normalized to the primitive mantle (McDonough and Sun, 1995). Colored lines show data
 5 from this study. Grey fields show mean value and 2σ range for representative lavas from
 6 nearby Galápagos volcanoes (symbols are consistent with previous figures; data sources
 7 as indicated in Fig. 4).
 8



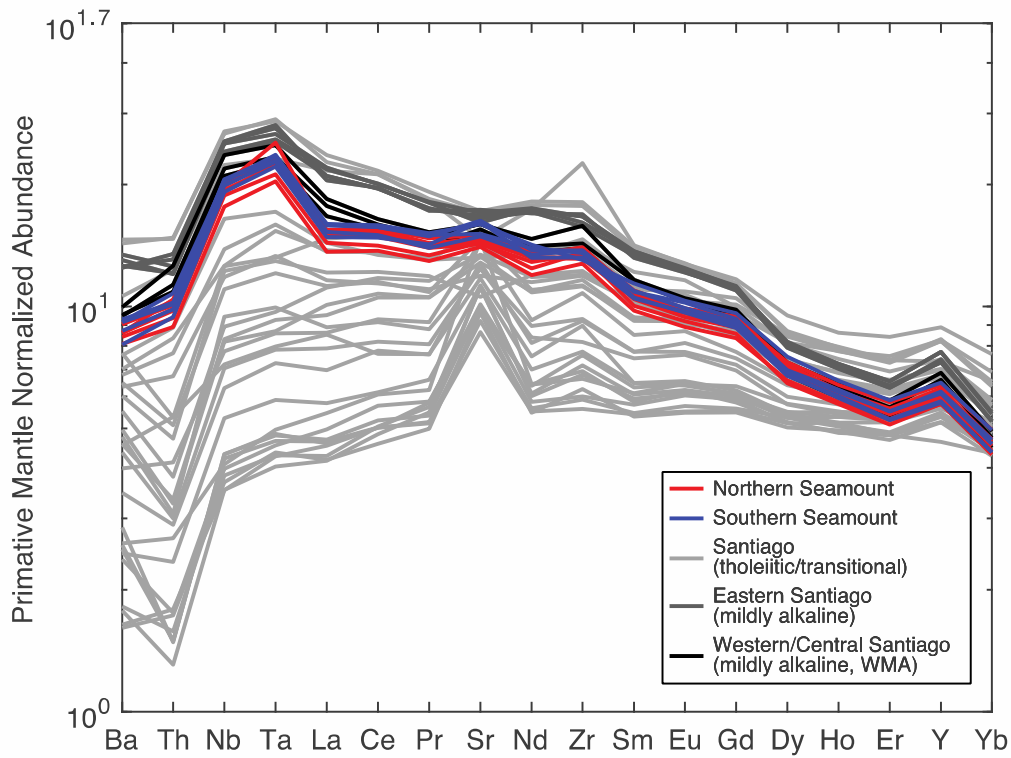
1
2 **Fig. 6: Variation of $[La/Sm]_N$ and $[La/Nb]_N$ as a Function of La Concentration** Trace
3 element ratios are normalized to CI (McDonough and Sun, 1995). Outlined colored
4 markers show data from this study. Grey markers show representative lavas from nearby
5 Galápagos volcanoes (data sources as indicated in Fig. 4).
6



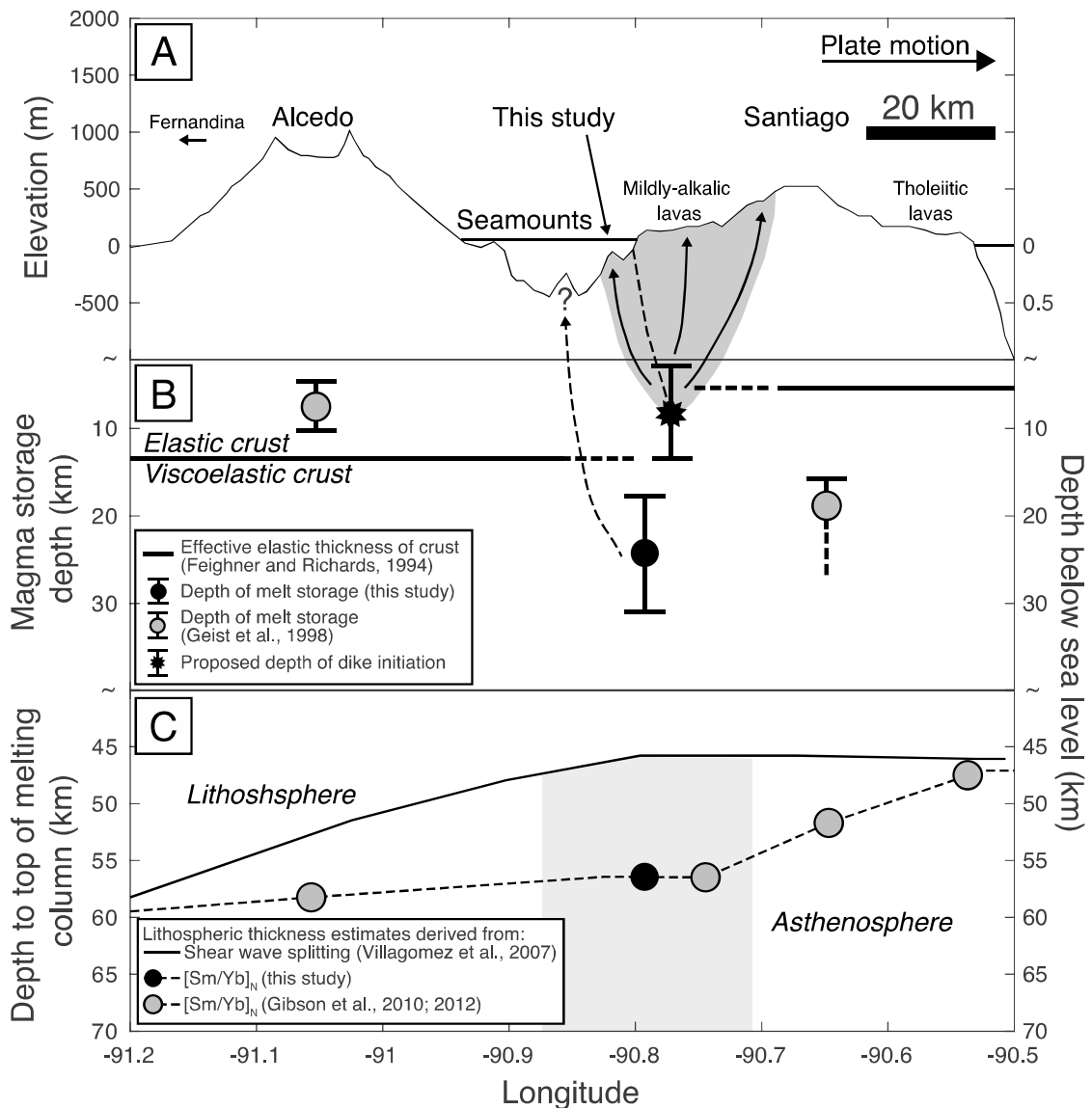
1
 2 **Fig. 7: REE Diagram Comparing the Seamount Samples to Averaged Galápagos**
 3 **Lavas** Elements are normalized to the primitive mantle (McDonough and Sun, 1995).
 4 Colored lines show data from this study. Grey fields show mean value and 2σ range for
 5 representative lavas from nearby Galápagos volcanoes (symbols are consistent with
 6 previous figures; data sources as indicated in Fig. 4).
 7



1
 2 **Fig. 8: Variation of $[Sm/Yb]_N$ as a Function of $[La/Sm]_N$** Trace element ratios are
 3 normalized to CI (McDonough and Sun, 1995). Outlined colored markers show data from
 4 this study. Grey markers show representative lavas from nearby Galápagos volcanoes
 5 (data sources as indicated in Fig. 4).
 6



1
 2 **Fig. 9: Trace Element Diagram Comparing the Seamount Samples to Santiago**
 3 **Lavas** Elements are listed in order of relative compatibility and normalized to the
 4 primitive mantle (McDonough and Sun, 1995). Colored lines show data from this study.
 5 Grey lines show Santiago lava compositions simplified from Gibson et al. (2012).
 6



1
2 **Fig. 10: Schematic Cross-Section Depicting Seamount Genesis** A) Thin black line is
3 an elevation profile from W-E across the Galápagos Platform, from Alcedo Volcano on
4 Isabela Island to Santiago Island. Thick black horizontal line shows sea level. Dark grey
5 region is the proposed extent of shallow diking, resulting in distribution of mildly alkalic
6 lavas from seamounts to central Santiago. Dashed line within the diking region indicates
7 a separation between the seamount lavas from those erupted subaerially. Solid arrows
8 indicate rapid melt transport in elastic crust evidenced by limited shallow degassing of
9 lavas (Sec. 5). Dashed arrow shows potential melt transport pathway for other unexplored
10 seamounts. B) Solid line is the effective elastic thickness of crust (Feighner and Richards,
11 1994). Black circle indicates range of melt storage and crystallization depths for
12 seamount lavas, derived from $\text{CaO}/\text{Al}_2\text{O}_3$ ratios (Sec. 5). Grey circles indicate range of
13 melt storage depths for Alcedo and Santiago (Geist et al., 1998). Black decagram
14 indicates depth of dike initiation constrained by transition into the elastic crust (6-12 km)
15 and depths derived from CO_2 and H_2O vapor saturation pressures (1.2 km; Sec. 5). C)

1 Solid black line indicates lithospheric thickness derived from shear wave splitting data
2 (Villagómez et al., 2007). Black circle indicates top of the melting column calculated
3 from average $[Sm/Yb]_N$ values of seamount samples from this study. Grey circles indicate
4 top of the melting column calculated from average $[Sm/Yb]_N$ values from Alcedo (Gibson
5 and Geist, 2010) and Santiago (Gibson et al., 2012). Black dashed line is the lithospheric
6 thickness derived from the combined $[Sm/Yb]_N$ calculations. Light grey region indicates
7 the potential melting region for seamount lavas.